ASME Turbo Expo
June 3-7, 2013, San Antonio, Texas

GT2013-94501

INVERSE AEROACOUSTIC DESIGN OF AXIAL FANS USING GENETIC OPTIMIZATION AND THE LATTICE-BOLTZMANN METHOD

Michael Stadler
NInsight
Graz, Austria

Michael B. Schmitz
ebm-papst St. Georgen
St. Georgen, Germany

Wolfgang Laufer
ebm-papst St. Georgen
St. Georgen, Germany

Peter Ragg
ebm-papst St. Georgen
St. Georgen, Germany

ABSTRACT

The noise emitted by axial fans plays an integral role in product design. When conventional design procedures are applied, aeroacoustic properties are controlled via an extensive trial-and-error process. This involves building physical prototypes and performing acoustic measurements. In general, this procedure makes it difficult for a designer to gain an understanding of the functional relationship between noise and geometrical parameters of the fan. Hence, it is difficult for a human designer to control the aeroacoustic properties of the fan.

To reduce the complexity of this process, we propose an inverse design methodology driven by a genetic algorithm. It aims to find the fan geometry for a set of given objectives. These include, most notably, the sound pressure frequency spectrum, aerodynamic efficiency, pressure head and flow rate. Individual bands of the sound pressure frequency spectrum may be controlled implicitly as a function of certain geometric parameters of the fan.

In keeping with inverse design theory, we represent the design of axial fans as a multi-objective, multi-parameter optimization problem. The individual geometric components of the fan (e.g., rotor blades, winglets, guide vanes, shroud and diffusor) are represented by free-form surfaces. In particular, each blade of the fan is parameterized individually. Hence, the resulting fan is composed of geometrically different blades. This approach is useful when studying noise reduction.

For the analysis of the flow field and associated objectives, we utilize a standard RANS solver. However, for the evaluation of the generated noise, a meshless Lattice-Boltzmann solver is employed. The method is demonstrated for a small axial fan, for which tonal noise is reduced.

NOMENCLATURE

N … number of blades	[1]
BPF_i … blade passing frequency of order i	[Hz]
n … rotational speed	[s^{-1}]
η … efficiency	[1]
L_w … sound power level	[dB]
p … static pressure	[Pa]
p_t … total pressure	[Pa]
$\dot{V}$ … flow rate	[m^3/s]
D … diameter of the fan	[m]
R … hub radius	[m]
R_{fh} … fillet radius for the hub	[m]
l_d … axial depth of the hub	[m]
ρ … density of air	[kg/m^3]
$\eta = p \cdot \dot{V}/(M \cdot \omega)$ … aerodynamic efficiency	[1]
$\varphi = 4\dot{V}/(\pi^2 D^3 n)$ … dimensionless flow rate	[1]
$\psi = 2\Delta p_t/(\pi^2 \rho D^2 n^2)$ … dimensionless pressure	[1]
f … objective function	[.]
$\tilde{f}$ … metamodel	[.]
γ … distance between turbulator and trailing edge	[mm]
σ … height of the turbulator step	[mm]

INTRODUCTION

Small axial fans are frequently used for ventilation in noise-sensitive environments. For example, in the IT industry, axial fans are utilized for cooling semiconductor equipment. Therefore, the reduction of associated noise emission has become a criterion of working ergonomics, in order to minimize employee hearing loss during long-term exposure. In addition, in the automotive industry, the introduction of automobiles propelled by electric motors will eliminate noise caused by combustion engines — making other noise sources (such as fans associated with the air conditioning system) more apparent to passengers. As a third example, in the design of energy-efficient housing, controlled ventilation via fans utilizes heat exchangers to reduce the carbon dioxide footprint of air-conditioning systems. In these industries, the reduction of noise emission from axial fans has become an important product marketing feature for many applications. To optimize personal comfort, many of these applications require exacting control of flow rates from axial fans. Hence, fan noise must be reduced for a range of off-design behaviors.

Noise generation is inherently difficult to control by a human designer, due to the complexity of the involved physical phenomena. For this reason, a simplification of the aeroacoustic design process is highly desirable. In a previous paper [26], we have demonstrated noise reduction for axial fans via genetic optimization of (a) the winglet geometry and (b) the turbulator for a fixed-blade geometry. In this paper, we take the approach one step further by demonstrating an inverse design methodology for the shape of the blades. Because each blade is treated individually, all blades of the fan may be loaded differently. The optimal blade loading is identified by a genetic algorithm.

This method accepts a number of objectives: the sound pressure frequency spectrum, aerodynamic efficiency, pressure head and flow rate. Based on multi-objective differential evolution, the method will then find the associated blade geometry.

The optimization is carried out for an axial fan with a diameter of 150 mm, consisting of seven blades (see Fig. 1) and operating at 7200 rpm. This fan is part of the new S-Force 2 family designed by ebm-papst.

For the sake of completeness, we will briefly review the results of our previous research (for more detailed information, refer to [26]):

Winglet. The winglet geometry represents a helical extrusion of the blade in the radial direction of the fan. In terms of parametric computer-aided design (CAD), this arrangement is obtained by cutting the blade with a cylinder with a diameter of $0.8\,D$, whose axis coincides with the fan axis χ (see Fig. 2). Thereby, D represents the outer diameter of the fan. We shall denote the resulting cross section by λ. Subsequently, a second cross-section μ is created by orthogonal projection of λ onto a cylindrical surface of diameter D and axis χ. For successive shape optimization, it is convenient to parameterize the transformations of μ in the following way:

(1) rotation about the radial axis ξ,
(2) rotation about the fan axis χ and
(3) translation along χ.

The closure of the winglet surface is obtained by a multi-section extrusion κ between sections λ and μ (thereby enforcing C^1 continuity at the interface between the original blade and κ; see Fig. 2).

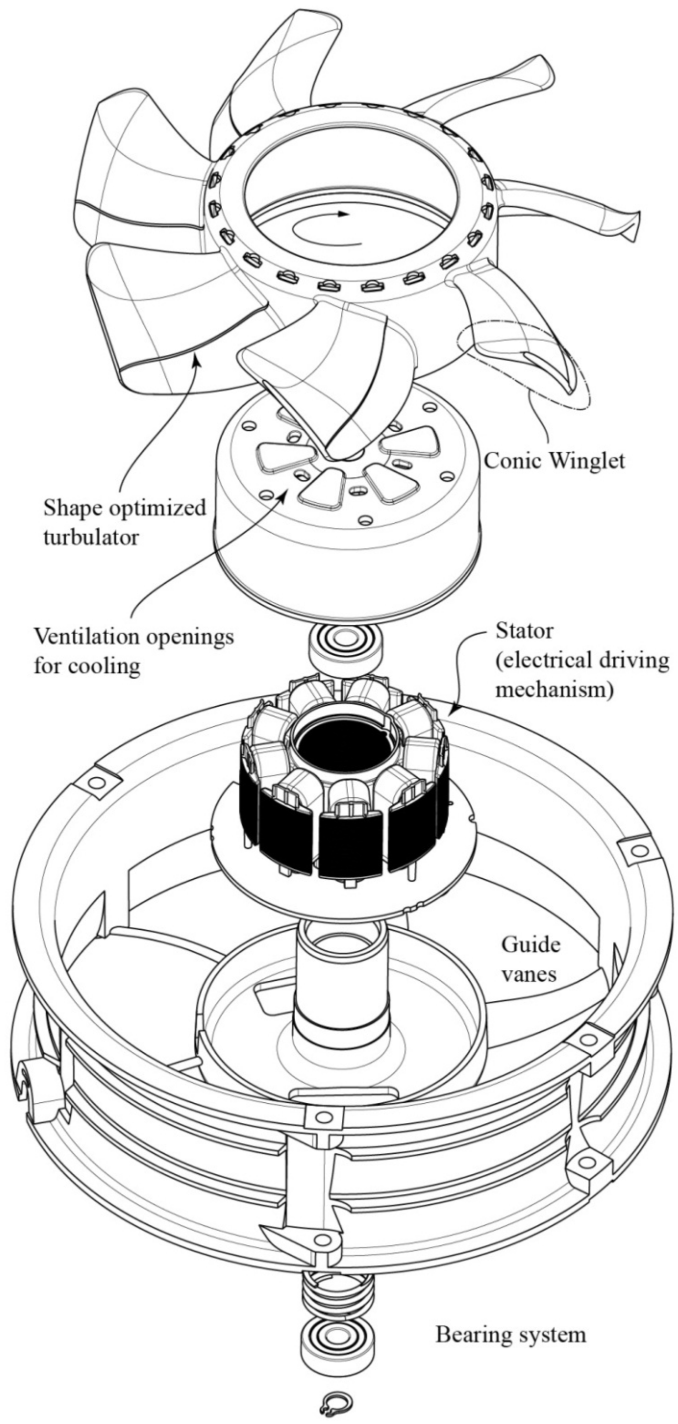

Fig. 1: Exploded view of the axial fan under investigation. The conical winglet design and the shape-optimized turbulator are indicated.

The optimized winglet geometry shows an interesting shape. It bends toward the suction side at the leading edge (angle α, Fig. 2) and toward the pressure side at the trailing edge (angle β, Fig. 2). The detailed winglet geometry can be observed in sections A to F in Fig. 2. The radius of curvature of the winglet varies along the blade. Hence, it resembles a number of generalized conical sections.

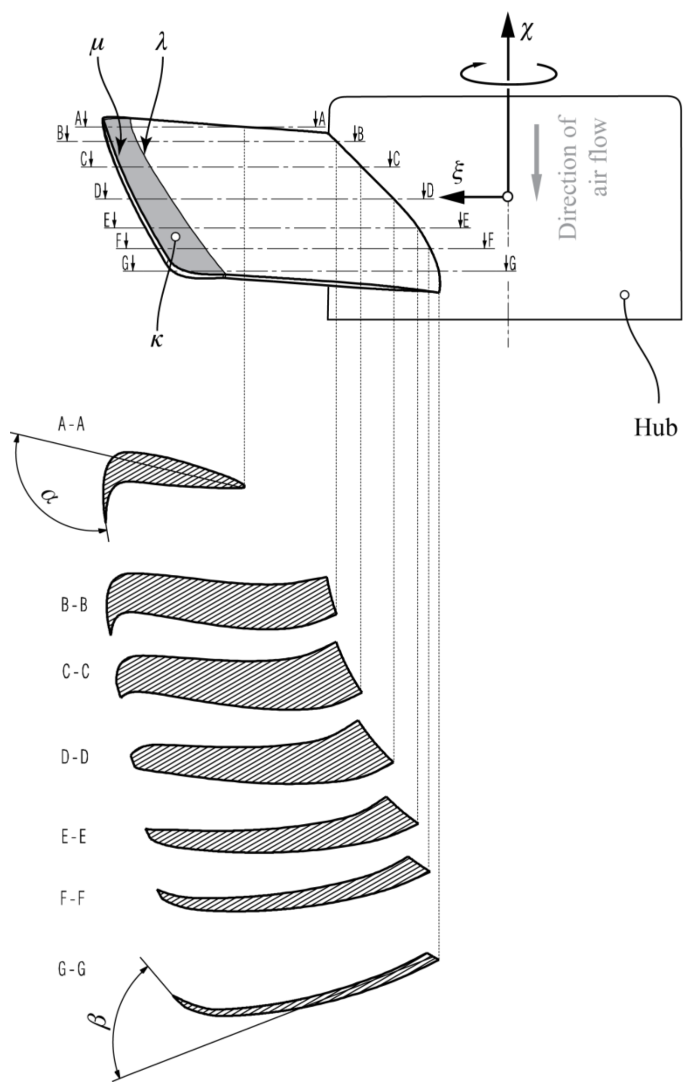

Fig. 2: Sections A-A to G-G (which are aligned normal to axis χ), illustrating the conical winglet geometry (only one blade is shown).

Turbulator. In general, turbulators are used to turn laminar flow into turbulent flow. However, turbulators can also be utilized to increase the energy of an already turbulent boundary layer, thereby moving the point of flow separation further downstream. This type of arrangement is used, for example, to avoid flow separation upstream of ailerons of commercial airliners.

At the leading edge of the blade, the flow will be laminar. After a certain distance, the flow will transition from laminar to turbulent. Further downstream (at the flow separation point), the turbulent boundary layer will break down due to the large positive pressure gradient near the end of the blade. This leads to undesirable effects, such as increased generation of noise and a reduced cross-sectional area for the flow channel. For off-design operating points of the fan, the point of flow separation travels further upstream, thereby exaggerating these negative flow characteristics even more. To avoid this, we have proposed a turbulator design as shown in Fig. 1.

The spine of the turbulator is represented by a B-spline, which is projected onto the blade surface. The cross-section of the turbulator is described as a simple step. In particular, we propose the following parameters:
(1) offset γ of B-spline control points between turbulator and trailing edge of the blade and
(2) height σ of the turbulator step.

This concludes the short review of our previous research. With the associated optimal configuration of the fan, the minimal sound power level of 82.2 dB was achieved (980 m³/h, 334 Pa, 7200 rpm, $\varphi = 0.277$).

This paper is structured as follows: first we outline the concept of *differential evolution* in order to set up the genetic algorithm. Then we illustrate the *parameterization of the blades*, taking into account that each blade is loaded differently. Subsequently, we outline the details of the *numerical simulation.* In the next section focusing on *inverse design of variable blade loading,* all components from the previous sections are assembled. Since the aeroacoustic analysis represents high computational loads, the *computational environment* is an issue in itself, which is outlined in a dedicated section. The accuracy of the numerical simulation is discussed in the section about the *experimental set-up.* In the final section, we present the *results* of our optimal load distribution for each individual blade, as well as the resulting noise reduction delivered by this fan design.

DIFFERENTIAL EVOLUTION

Evolution Algorithms (EA) have been proposed in the seminal papers [11] and [12]. According to Darwinian concepts of evolution, populations of individuals evolve over a search space, adapting to the environment via the use of different strategies such as selection, mutation and crossover. The fitness of individuals — which can be represented by evolution algorithms — increases their chance to survive and reproduce.

With regard to design optimization problems, EAs exhibit a number of advantages over traditional gradient-based methods:

- the objective function does not need to be continuous,
- there is an insensitivity to noise caused by the objective function (i.e., global minima will be found in the presence of local minima) and

- EA methods are easily adaptable to parallel computing platforms.

However, EAs involve a large number of function evaluations which may be considered a disadvantage.

Differential Evolution (DE) represents an evolutionary method that was developed more recently [13]. Like all EAs, it is based on populations which are composed of individuals, each of them described by a design vector $\mathbf{x}_t = (x_1, x_2, \dots, x_m)$ for generation t, containing m parameters. During each generation, the complete population of design vectors must be evaluated.

For the evolution of design vector $\mathbf{x}_t$, the processes of mutation, recombination and selection are performed successively:

Mutation is performed by randomly choosing three unique parameter vectors $\mathbf{a}_t, \mathbf{b}_t$ and $\mathbf{c}_t$ according to $\mathbf{a}_t \neq \mathbf{b}_t \neq \mathbf{c}_t \neq \mathbf{x}_t$ to form the new trial vector

$$\mathbf{y}_t = \mathbf{a}_t + F \cdot (\mathbf{b}_t - \mathbf{c}_t) \tag{1}$$

Thereby, $F \in]0,2[$ is a user-specified constant which controls the amplification of the differential variation $(\mathbf{b}_t - \mathbf{c}_t)$.

Recombination is the breaking and rejoining of DNA strands to encode novel sets of genetic information. Mathematically, it may be represented by definition of the candidate vector $\mathbf{z}_t = (z_1, z_2, \dots, z_m)$ as

$$z_i = \begin{cases} y_i & \text{if} \quad r_i \le C \\ x_i & \text{if} \quad r_i > C \end{cases} \quad i = 1 \dots m \tag{2}$$

where r_i is a uniformly distributed random variable $(0 \le r_i < 1)$ and $C \in]0,1[$ represents a user-defined constant.

Selection helps to minimize the objective function $f(\mathbf{x}_t)$ according to

$$\mathbf{x}_{t+1} = \begin{cases} \mathbf{z}_t & \text{if} \quad f(\mathbf{z}_t) \le f(\mathbf{x}_t) \\ \mathbf{x}_t & \text{if} \quad f(\mathbf{z}_t) > f(\mathbf{x}_t) \end{cases} \tag{3}$$

The methods described above refer to single-objective differential evolution. However, in the context of fan optimization, we require the simultaneous optimization of more than one objective (e.g., aerodynamic efficiency must be optimized along with noise production). Hence, the concepts described above must be extended to multi-objective differential evolution. This was first introduced in [14] by restricting the selection of the individuals $\mathbf{a}_t, \mathbf{b}_t$ and $\mathbf{c}_t$ to the non-dominated individuals. Hence, $\mathbf{a}_t \neq \mathbf{b}_t \neq \mathbf{c}_t$ are required to belong to the Pareto front.

Another approach was described in [15] and [16]: for each generation, all newly created individuals generated by mutation and recombination are added to the population. Therefore, the resulting population is twice as large and is subjected to a non-dominated ranking procedure. This method selects all non-dominated individuals, assigns them rank 1 and removes them from the population. Successively, the ranking procedure is repeated to identify individuals of higher ranks until the whole population is ranked. In a final step, the original size of the population is obtained by adding individuals from ranks of increasing number, starting from rank 1. These strategies form the core of NSGA-II [16].

A major drawback of the methods described above is the large number of objective function evaluations. In particular, for aeroacoustic simulations, they may become prohibitively expensive. To reduce the computational workload, the numerically intensive computations can be replaced by cheaper evaluations, or even interpolations between accurately evaluated objective functions of individuals. These techniques are known as *metamodel assisted evolutionary algorithms*. A metamodel is a function $\tilde{f}(\boldsymbol{x}): \mathbb{R}^u \to \mathbb{R}^v$ with a much lower computational cost than $f(\mathbf{x})$ such that

$$\left\| \tilde{f}(\mathbf{x}) - f(\mathbf{x}) \right\| < \epsilon \tag{4}$$

where ϵ is sufficiently small. Metamodels may be categorized into *on-line* and *off-line* trained metamodels.

The *on-line* methods utilize the metamodel for some or all of the individuals making up the population. After the ranking procedure, the most promising individuals are reevaluated using the accurate objective function (for example, see [17] and [18]).

In contrast, the *off-line* methods use the metamodel during the entire evolutionary process. Only at the end of the evolution, the most successful individuals are reevaluated using the accurate objective function (for example, see [19] and [20]). It is beneficial to integrate these individuals into the metamodel for subsequent evolutions in order to facilitate self-learning.

Metamodels may be set up in a number of ways. Among them are the

- Polynomial Response Surface Models (PRSMs),
- Artificial Neural Networks (ANNs),
- Radial Basis Function (RBF) networks and
- Kriging.

These will be reviewed in more detail in a later section.

PRSMs aim to represent $\tilde{f}$ by quadratic or cubic polynomials (see [21], among others). Hence, an advantage of PRSMs is that the minimum may be found by analytical derivation and application of the Newton-Raphson method. However, polynomial basis functions have proven to be inferior in representing f for aerodynamic applications.

An ANN consists of a network of neurons which are arranged in layers: an input layer, one or more hidden layers and an output layer. Each element of the input layer is connected to each neuron of the first hidden layer. Each of these connections is associated with a weight. What distinguishes ANNs from regression techniques such as RSM is the Kolmogorov Theorem. It states that any continuous function $f(\boldsymbol{x}): \mathbb{R}^u \to \mathbb{R}^v$ can be represented exactly by a three-layer, feed-forward neural network with u elements in the input layer, $2u + 1$ elements in the hidden layer, and v elements in the output layer. ANNs were originally developed to imitate brain functions. However, they also represent powerful interpolation functions (see [22], among others). Before the network can be used for interpolation, it must be exposed to a training phase based on error back-propagation.

RBF networks belong to the same class of interpolators as ANNs. However, they have a different architecture and input-to-output relationship. Each hidden neuron has an m-dimensional input (as opposed to the 1D weighted sum of the input variables for ANNs).

Kriging (see [24], among others) belongs to the group of least-square algorithms, although it reproduces source data exactly (i.e., $\tilde{f}(\boldsymbol{x}_i) = f(\boldsymbol{x}_i)$). In addition to the prediction of the objective function, this method also supplies an estimation of the error of the prediction. This feature was originally utilized in geostatistics. However, recently it has grown in popularity for the approximation of deterministic computer models.

Within this research, we focus on inverse aeroacoustic design. This involves the evaluation of numerically expensive objective functions based on Lattice-Boltzmann models. Hence, for numerical efficiency it is mandatory to augment the evolution process with a metamodel. Due to the nonlinearity of the problem, the PRSM led to unsatisfactory convergence. For the efficient solution of the problem, we have developed an NSGA-II based evolution algorithm, augmented with an off-line trained metamodel, which is supported by a radial basis function network. This approach is illustrated in Fig. 3.

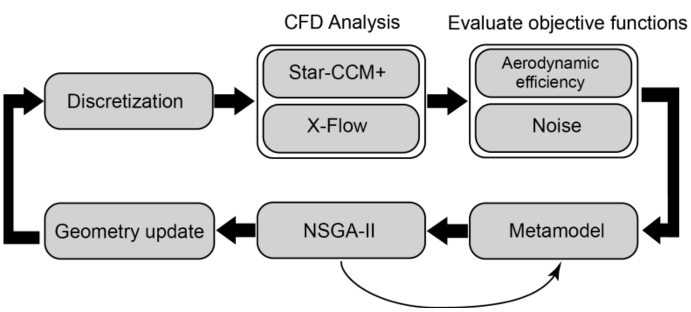

Fig. 3: *Flowchart of the inverse design algorithm.*

PARAMETERIZATION OF THE BLADE GEOMETRY

As a general rule, to make the inverse design procedure more efficient, a few guidelines should be adhered to:

- the number of geometric parameters should be minimized and
- the design space should be set up to exclude physically impossible designs.

Based on these guidelines, the individual parts of the fan were parameterized.

For the parameterization of the blade, we describe the skeletal surface by sheets of vorticity according to [27]. Their strength is determined by a user-specified distribution of circumferentially averaged swirl velocity ($r \cdot \bar{c_u}$), defined as

$$r \cdot \bar{c_u} = \frac{N}{2\pi} \int_0^{\frac{2\pi}{N}} r \cdot c_u d\theta \tag{5}$$

where N is the number of blades, r is the radius, c_u is the circumferential velocity component and θ is the angular coordinate in the cylindrical coordinate system. The blade loading is directly related to the meridional derivatives of $r \cdot \bar{c_u}$, hence

$$\Delta p = \frac{2\pi}{N} \rho w_{mbl} \frac{\partial (r \cdot \bar{c_u})}{\partial m} \tag{6}$$

where Δp is the pressure loading on the blade, w_{mbl} is the relative meridional blade surface velocity and ∂m refers to a derivative in the meridional plane. The blade shape is obtained by alignment of its skeletal surface with the local velocity vector (i.e., imposing the inviscid slip condition). Consequently, the blade shape is controlled by a few parameters which define the distribution of $r \cdot \bar{c_u}$ across the meridional section. This helps to greatly reduce the number of parameters describing the blade (as opposed to describing the blade geometry directly by a B-spline surface with associated control points as parameters). In addition, it precludes many non-physical blade geometries. (For more details, see [27].) The thickness of the blade is defined by a NACA profile.

NUMERICAL SIMULATION

Numerical simulation of the fluid dynamics was carried out mainly in Star-CCM+ V6.04 [2], using its classical Reynolds Averaged Navier Stokes (RANS) solver which is based on a polyhedral discretization scheme. Turbulent flow was resolved using the realizable two-layer k-ε turbulence model, as well as the integrated two-layer all y+ wall model [2]. To resolve the fine details of the geometry, a segment of the fan (i.e., 1/7th of the full model) was discretized by approximately 1,500,000 polyhedral and prismatic cells.

To perform numerical analysis of the acoustic performance of the fan, we used the Lattice-Boltzmann code XFlow [1]. It represents a proprietary, particle-based, meshless approach which aims to solve complex problems on relatively standard computer hardware. It features a novel, particle-based, kinetic algorithm that resolves both the Boltzmann and the compressible Navier-Stokes equations. Furthermore, it provides state-of-the-art Large Eddy Simulation (LES) modeling and advanced non-equilibrium wall models. These features make it attractive for direct acoustic analysis within our optimization framework.

XFlow has been benchmarked for a number of standard fluid dynamics problems in [4]. In addition, we have performed a series of benchmark analyses for basic engineering problems (cylinder in cross-flow), as well as for axial fans. These results were consistent with experimental data (see [5]-[7]). More information about the details of the method can be found in our recent paper [26]. The geometric model is shown in Fig. 4.

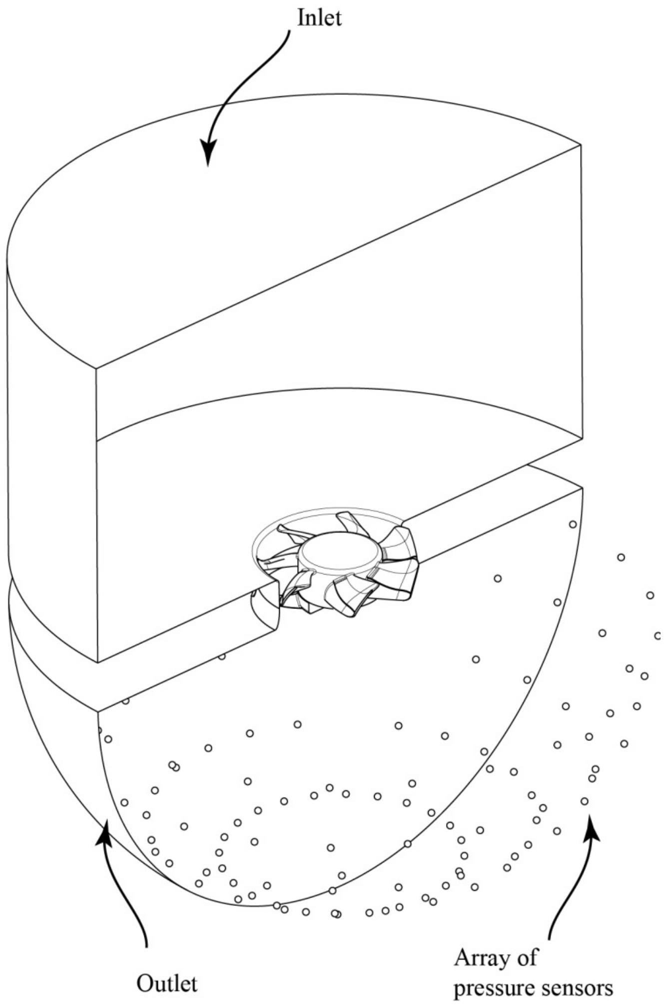

Fig. 4: Geometric model for the Lattice-Boltzmann simulation showing inlet, outlet, the fan under investigation and the array of pressure sensors (the sensors are only shown at the outlet).

INVERSE DESIGN OF VARIABLE BLADE LOADING

At this point, we have introduced all necessary prerequisites. We will now assemble these components into an inverse design strategy that can effectively be applied to axial fans. The objectives are

- to maximize aerodynamic efficiency (f_1) and
- to minimize the sound pressure level (f_2).

The objective function for aerodynamic efficiency

$$\eta = \frac{\Delta p \dot{V}}{M\omega} \tag{7}$$

can be written as

$$f_1 = \max(\eta). \tag{8}$$

The second objective function is associated with sound pressure. It is written implicitly as a function of frequency by involving a number r of selected bands of the sound-pressure frequency spectrum. Hence,

$$f_2 = \min\left(10 \log \sum_{i=1}^{r} 10^{(L_p)_i - (L_A)_i}\right) \tag{9}$$

Thereby, $\left(L_p\right)_i$ refers to the sound pressure of the frequency band with index i, and $(L_A)_i$ refers to the associated A-weighting. This approach helps to control the set of particular bands during the inverse design procedure. By choosing the band frequencies as multiples of $N \cdot n$, this enables us to bias the objective function for reduction of tonal over broadband noise. This distinction is important in many noise-reduction applications.

Tonal noise of an axial fan is considered to be most unpleasant to human ears. It is caused by transient pressure fluctuations due to the passage of N identical blades. Within the sound-pressure frequency spectrum, the blade passing frequency of order i is represented by a peak at $\mathrm{BPF}_i = i\, N\, n$. Several strategies have been developed to alleviate these peaks, most notably the variable angular alignment of blades. This alignment spreads acoustic energy over a small spectrum of frequencies, and as a result the amplitude of the peaks is slightly reduced.

We choose a different strategy by specifying a fan which consists of N differently designed blades. In this case, each flow channel constitutes different flow characteristics. In theory, this should help to reduce tonal noise even further. However, whether geometrically different blades actually deliver noise-reduction benefits remains an open question. The answer may be found by applying evolution algorithms.

To set up this evolutionary problem, each of the N blades is parameterized individually. In particular, we choose to parameterize the averaged swirl velocity $r \cdot \overline{c_u}$ at the following locations:

- trailing edge / hub and
- trailing edge / shroud

At the leading edge, we set $r \cdot \overline{c_u} = 0$. Between these locations, $r \cdot \overline{c_u}$ is interpolated linearly. Consequently, the number of parameters describing the problem is $2 \cdot N$.

COMPUTATIONAL ENVIRONMENT

The evolution algorithm requires a large number of objective function evaluations. These evaluations are numerically expensive, since they involve the solution of the Lattice-Boltzmann model. Throughout the inverse design procedure, the number of individuals making up the population is varied dynamically by the evolution algorithm. These requirements cannot be satisfied efficiently by a standard computer cluster, since it cannot expand or shrink the available resources easily. However, Amazon Elastic Compute Cloud

(EC2) [28] is a web service that provides resizable compute capacity in the cloud. It enables users to increase or decrease capacity within minutes. In contrast, standard cluster services may require several days until they can adapt their resources. This would not be acceptable during an inverse design run.

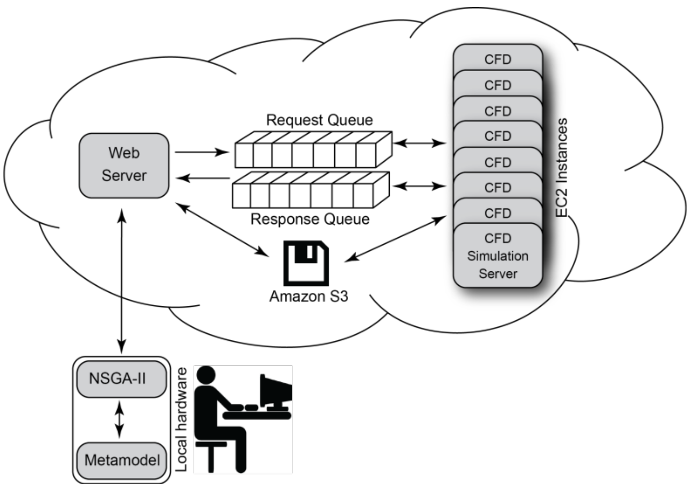

Fig. 5: Structure of parallel computing resources on Amazon Elastic Compute Cloud (EC2).

EC2 works in conjunction with Amazon Simple Storage Service (Amazon S3) and other services to provide a complete solution for large-scale computing. The structure for incorporating EC2 into the evolution method is illustrated in Fig. 5. Both the control algorithm (NSGA-II), as well as the evaluation of the metamodel, can be executed on standard desktop hardware, since these operations are numerically cheap.

The control algorithm NSGA-II is configured to communicate with a web server in the cloud. Whenever it determines that an accurate evaluation of an objective function is necessary, it passes the associated parameters (including the geometry) to the web server. A dedicated request for the numerical analysis is put into the request queue. As soon as EC2 can provide the necessary computing resources, the analysis is initiated in parallel on a number of dedicated CFD simulation servers.

A CFD simulation server is represented by a virtual image of an operating system, with associated simulation programs. These programs may be run from the web server via a command shell.

During a simulation run, all results remain on the file server (Amazon S3). The objective functions are then evaluated on the CFD simulation server, and this result is supplied to the web server via the response queue. The data generated by a Lattice-Boltzmann analysis may reach several gigabytes. However, the result of the objective function may only be a few floating point values which describe aerodynamic efficiency, as well as the individual bands of the sound-pressure frequency spectrum. Hence, only very small sets of data need to be transferred over the internet between the cloud service and the local hardware. This helps to increase the efficiency of the computational environment.

For the present study, we have utilized EC2 cloud configurations consisting of 128 CPUs. A total of 300 geometric configurations were analyzed. The number of analyses done in parallel was controlled by NSGA-II, varying between 5 and 20.

EXPERIMENTAL SET-UP

From experiments, we obtained fan charts and the associated sound power levels. To facilitate testing of arbitrary configurations, a modular test set-up was designed, consisting of the following four fan components: (1) casing, (2) impeller, (3) guide vanes and (4) inlet nozzle. Each of these components can be changed individually to study its specific influence on overall performance. A typical set-up is shown in Fig. 6. The components (2)-(4) are made by rapid prototyping.

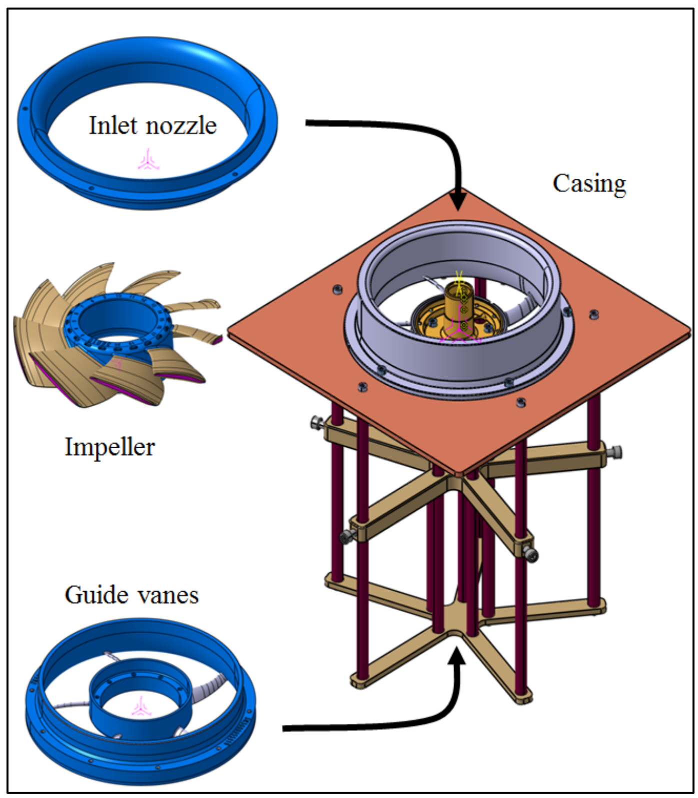

Fig. 6: Experimental set-up.

The aerodynamic testing rig (see Fig. 7) is a suction side throttled facility. When the test set-up is mounted at the exit of the testing rig, the air enters the rig through five tubes (see top of Fig. 7), each equipped with a flow meter. The air is conditioned with screens and gazes to ensure homogeneous flow at the fan inlet. An auxiliary fan compensates for the inherent pressure drop throughout the system. Fan charts are obtained by recording flow rate, as well as the difference between static pressure at the inlet and ambient pressure.

Fig. 7: Aerodynamic testing rig.

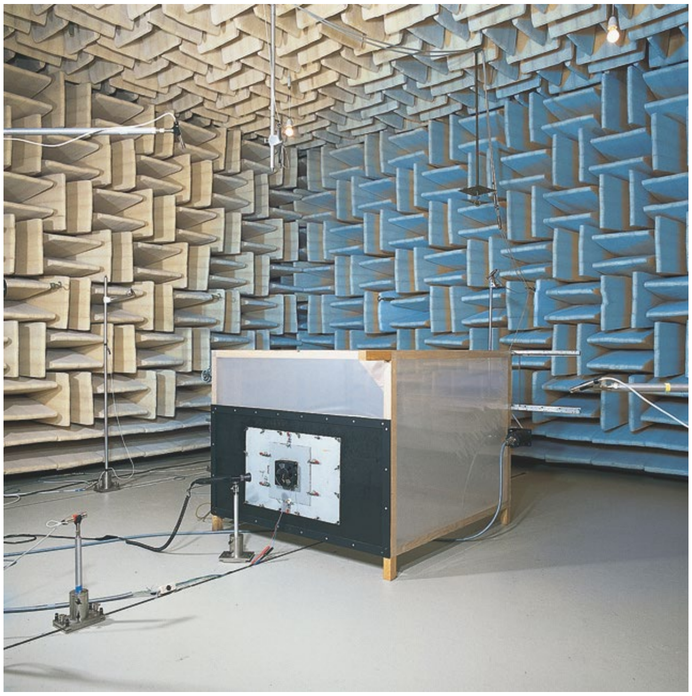

Fig. 8: Acoustic testing rig.

The acoustic testing rig (see Fig. 8) operates via throttling on the pressure side. The total sound power is computed according to ISO 10302, with 10 microphones placed on a hemisphere with a diameter of 2 m. (More details about the experimental set-up can be found in [3].)

RESULTS

To conclude the study, we describe the optimal parameter set obtained from the evolution algorithm. In addition, we illustrate the agreement between the results of the LBM simulation and physical tests. Finally, the improved performance of the fan due to the design optimization is documented.

Optimal parameter set. Since we have posed a multi-objective optimization problem (minimize sound-pressure levels while maximizing aerodynamic efficiency), the evolution algorithm produces a complete Pareto front of optimal designs. Clearly, the Pareto front is discontinuous. This may be caused by the nonlinear effects which appear at the guide vanes for increasing the variation in blade loading (i.e., neutral guide vanes suddenly become aerodynamically active for certain flow channels of the fan).

The entire population of individuals included in the optimization process is depicted in Fig. 9. The convergence of the proposed cooperation between NSGA-II and the radial basis function metamodel seems satisfactory, which is illustrated by the density gradient of dots shown in Fig. 9. To start the evolution, an initial parameter set was chosen which describes the fan developed in our recent paper [26], whose blades have identical geometry. Hence, the evolution began at a level of optimization that was already high.

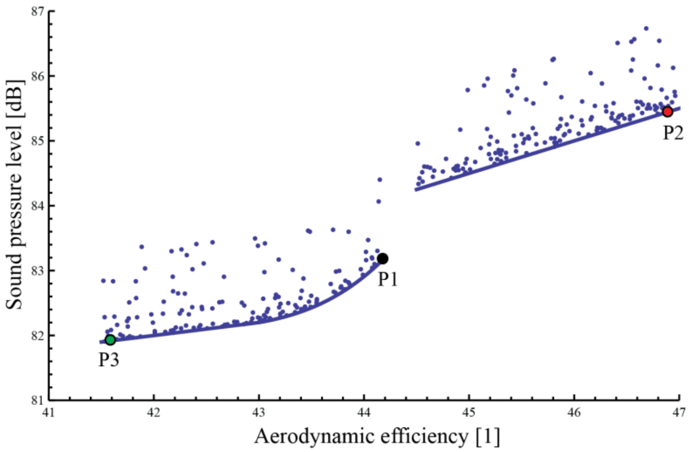

Fig. 9: Population of individuals chosen for evaluation by the NSGA-II algorithm. The Pareto front of optimal designs is discontinuous. Three individuals — P1, P2 and P3 — are chosen for subsequent study.

From the Pareto set of optimal designs, we have chosen to physically build one of them for further analysis. The individual was chosen from the center of the Pareto optimal solutions (see the black dot denoted by P1 in Fig. 9). The associated solution parameters for three individuals — P1, P2 and P3 — are shown in Fig. 10.

Spatial distribution of noise, based on LBM simulation. The emission of fan noise is not distributed uniformly around the fan. Hence, to study noise-generation phenomena, it makes sense to investigate the spatial distribution of noise sources. Otherwise, interesting effects might be hidden or obscured due to integration over the whole domain.

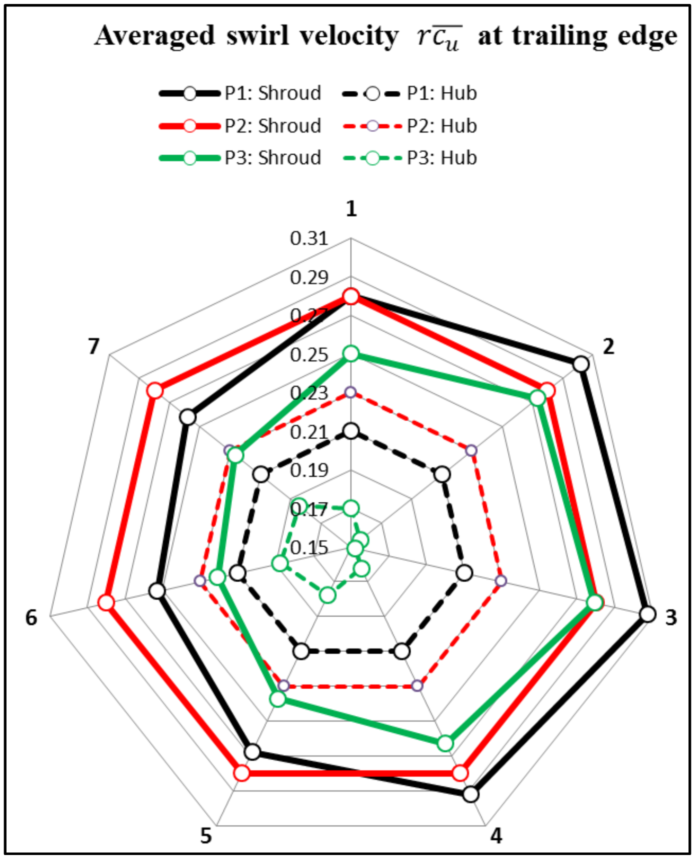

Fig. 10: Parameters for three selected individuals of the Pareto front. Individual P1 was selected from the center of the Pareto front in Fig. 9. The individuals P2 (aerodynamic efficiency more important than noise reduction) and P3 (noise reduction more important than aerodynamic efficiency) were selected from the peripheral regions of the Pareto front.

From the LBM simulation, we obtain the pressure distribution over time for a number of sensors (which are shown in Fig. 4). Via Fast Fourier Transform (FFT), the pressure data is converted to the frequency domain. For one of the sensors, the sound pressure level is shown in Fig. 11. It compares the fan of identical blade geometry (blue) to the fan of varying blade geometry (red). Clearly, for the fan with identical blade geometry, there are a number of blade-passing frequencies, represented by peaks. For the fan with varying blade geometry, these peaks are almost absent. Hence, tonal noise is reduced effectively by the evolution algorithm. However, it should be noted that the data shown in Fig. 11 represents an extreme example (for sensors at different locations, the difference between the two fan designs is less pronounced).

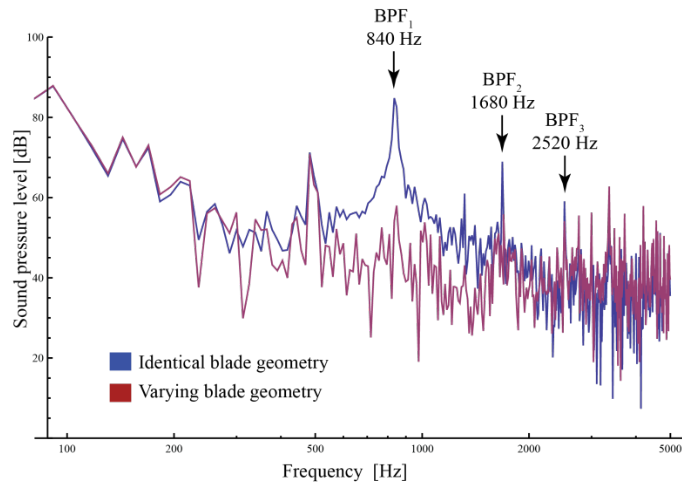

Fig. 11: Typical frequency spectrum of sound-pressure levels obtained from the Lattice-Boltzmann simulation for one of the sensors at the outlet. Blade-passing frequencies (BPF) up to order three are indicated.

Accuracy of the aeroacoustic simulation. To illustrate the accuracy of the numerical simulation, we show the frequency spectrum of emitted noise as 1/3-octave bands for the optimized fan design with varying blade geometry, operating at the design point. Then we compare this with tests on a physical specimen of the same fan. The overall agreement between simulation and physical test is within $\pm 2\text{dB}$ for most of the bands (see Fig. 12). This is satisfactory for the present application.

There are a few interesting results to discuss. For example, the peak at BPF$_1$ is clearly visible in the frequency spectrum for both the physical test and the numerical simulation (see the 800 Hz band in Fig. 12).

In contrast, for the physical test, another peak is observed at the rotational frequency $RF = 7200/60 = 120\,\text{Hz}$ which cannot be observed in the simulation. This peak is attributed to imperfect rotordynamics or eccentricity of the individual fan. The absence of this peak in the numerical simulation represents an advantage, since the frequency spectrum (and consequently, the objective function for the evolution algorithm) is not tainted by effects that are unrelated to aerodynamics. If such effects were included in the analysis, the evolution algorithm would be misguided.

Improvement over identical blade geometry. We compare two physical fan specimens: (1) the fan with identical blade geometry (developed in [26]) and (2) the fan with varying blade geometry (developed in the present paper). The frequency spectrum of fan noise is shown as 1/3-octave bands for the two fans in Fig. 13.

A few interesting aspects are visible: clearly, the peak at the first order blade-passing frequency $\text{BPF}_1 = 7200/60 * 7 =$

840 Hz is lower, and acoustic energy is distributed to adjacent frequencies (see circle 1 in Fig. 13). Furthermore, the peak at the second order blade-passing frequency $\mathrm{BPF}_2 = 2 * \mathrm{BPF}_1 = 1680$ Hz has almost disappeared (see circle 2 in Fig. 13). We also note that broadband noise is slightly reduced for the varying blade geometry. The total reduction of sound power level is 1.3 dB(A).

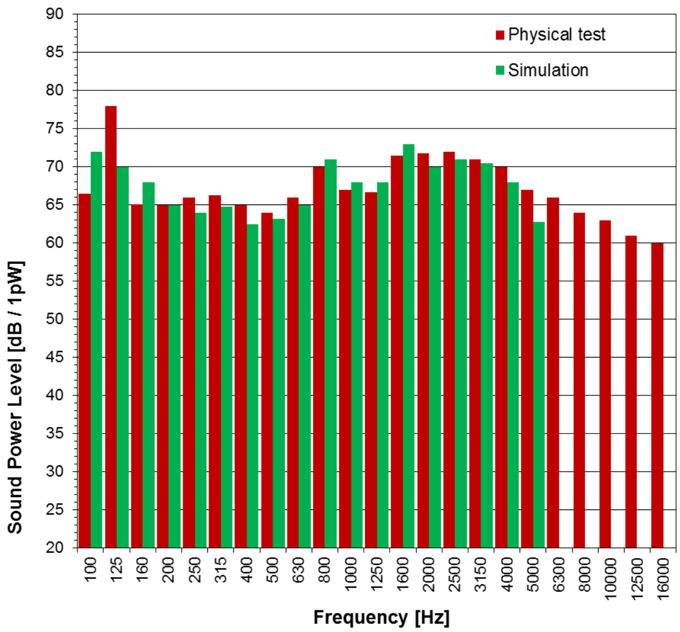

Fig. 12: Comparison between physical test and simulation for the fan with varying blade geometry. The frequency spectrum of fan noise is shown as 1/3-octave bands for the optimized fan operating at the design point. Measurements for a physical test (red) are compared with results from a numerical simulation (green) based on direct acoustic analysis via the Lattice-Boltzmann method. The time resolution of the simulation was $\Delta t = 10^{-4}$ s. Hence, in accordance with the Nyquist-Shannon sampling theorem, numerical results are limited up to a frequency of 5000 Hz. The peak for the physical test at 125 Hz is attributed to the eccentricity of the individual fan and therefore cannot be observed in the simulation.

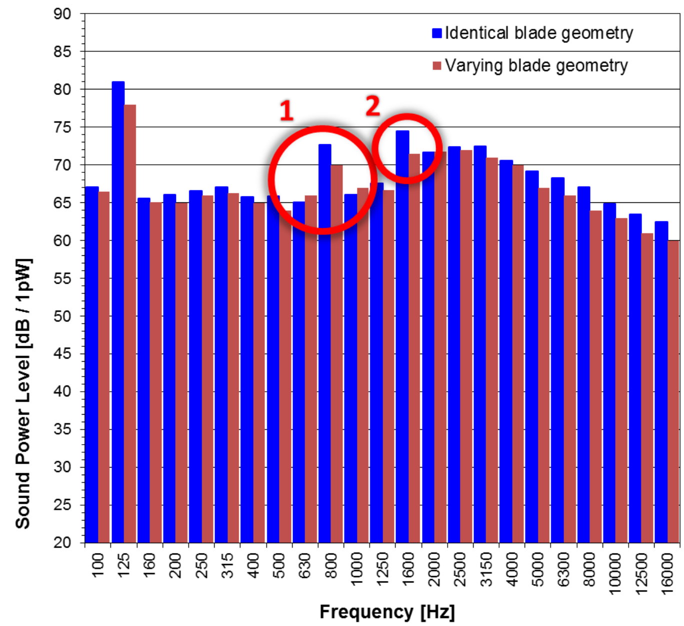

Fig. 13: Comparison of two physical specimens: The frequency spectrum of fan noise is shown as 1/3-octave bands for the fan with identical blades (blue) and for the fan with varying blade geometry (red). Clearly, the peak at BPF_1 is reduced and acoustic energy is distributed to adjacent frequencies (circle 1). The peak at BPF_2 has almost disappeared (circle 2). The overall reduction in sound power level is 1.3 dB(A).

ACKNOWLEDGEMENTS

The authors would like to thank G. Eimer and his team for performing the experiments and ebm-papst St. Georgen GmbH for supporting this study.

REFERENCES

[1] XFlow user manual. Next Limit Inc., 2011.
[2] Star CCM+ user manual. CD-Adapco, 2011.
[3] M.B. Schmitz, G. Eimer and H. Schmid. *Design and test of a small high performance diagonal fan*. Proceedings of ASME Turbo Expo 2011.
[4] XFlow Validation Guide. Next Limit Inc., 2011.
[5] V. Strouhal, “Über eine besondere Art der Tonerregung.” Annu. Phys. Chem. Vol. 5, pp. 216-251, 1878.
[6] H. Oertel Jr., *Wakes behind blunt bodies*, Annu. Rev. Fluid Mech. Vol. 22, pp. 539-564, 1990.
[7] C.H.K. Williamson, *Vortex dynamics in the cylinder wake*, Annu. Rev. Fluid Mech. Vol. 28, pp. 477-539, 1996.
[8] B. Chopard and M. Droz, *Cellular Automata Modeling of Physical Systems*, Cambridge University Press, 1998.
[9] U. Frisch, B. Hasslacher and Y. Pomeau, *Lattice-Gas Automata for the Navier-Stokes Equation*, Phys. Rev. Lett. 56, 1505-1508 (1986).

[10] G.R. McNamara and G. Zanetti, *Use of the Boltzmann Equation to Simulate Lattice-Gas Automata,* Phys. Rev. Lett. 61, 2332-2335 (1988).

[11] J.H. Holland, *Adaption in Natural and Artificial Systems.* University of Michigan Press, 1975.

[12] I. Rechenberg. *Evolutionsstrategie – Optimierung technischer Systeme nach Prinzipien der biologischen Evolution.* Fommann-Holzboog, Stuttgart, 1973.

[13] K. Price and N. Storn. *Differential Evolution.* Dr. Dobb's Journal, pp. 18-14, April 1997.

[14] H.A. Abbas, R. Sarker and C. Newton, *PDE: A Pareto-Frontier Differential Evolution Approach for Multi-Objective Optimization Problems.* In *Proceedings of the Congress on Evolutionary Computation,* Volume 2, pp. 971-978, Piscataway, New Jersey, 2001.

[15] N.K. Madavan, *Multiobjective Optimization using a Pareto Differential Evolution Approach.* In *Proceedings of the Congress on Evolutionary Computation*, Volume 2, pp. 1145-1150, Honolulu, Hawaii, 2002.

[16] K. Deb, S. Agrawal, A. Pratap and T. Meyarivan, *A fast elitist Non-Dominated Sorting Genetic Algorithm for Multi-Objective Optimization: NSGA-II.* In *Proceedings of the Parallel Problem Solving from Nature VI Conference,* pp. 849-858, Paris, France, 2000.

[17] K.C. Giannakoglou and M.K. Karakasis, *Hierarchical and Distributed Metamodel-Assisted Evolutionary Algorithms,* In *VKI Lecture Series on Introduction to Optimization and Multidisciplinary Design,* Brussels, March 2006.

[18] M.K. Karakasis, K.C. Giannakoglou and D.G. Koubogiannis, *Aerodynamic Design of Compressor Airfoils using Hierarchical, Distributed Metamodel-Assisted Evolutionary Algorithms,* In *7th European Conference on Turbomachinery, Fluid Dynamics and Thermodynamics,* Athens, 2007.

[19] S. Pierret, *Designing Turbo machinery Blades by means of the Function Approximation Concept based on Artificial Neural Network, Genetic Algorithm and the Navier-Stokes Equations.* Ph.D. Thesis, Faculte Polytechnique de Mons, December 1999.

[20] T. Verstraete, *Multidisciplinary Turbo machinery Component Optimization Considering Performance, Stress and Internal Heat Transfer.* Ph.D. Thesis, University of Ghent, June 2008.

[21] R.H. Myers and D.C. Montgomery, *Response Surface Methodology: Process and Product Optimization Using Designed Experiments.* Wiley, New York, 1995.

[22] H. White, R.A. Gallant, K. Kornik, M. Stinchcombe and J. Woolridge, *Artificial Neural Networks: approximation theory and learning.* Blackwell publishers, 1992.

[23] S. Haykin. *Neural Networks: A Comprehensive Foundation.* Prentice Hall, New Jersey, 1999.

[24] J.D. Martin and T.W. Simpson, *Use of Kriging Models to Approximate Deterministic Computer Models,* IAAA Journal, 43(4):853-863, 2005.

[25] A.G. Bors, *Introduction of the Radial Basis Function Networks*, Online Symposium for Electronics Engineers, 1(1), DSP Algorithms: Multimedia, Feb. 13 2001, pp. 1-7.

[26] M. Stadler, M.B. Schmitz, P. Ragg, D.M. Holman and R. Brionnaud, *Aeroacoustic Optimization for Axial Fans with the Lattice-Boltzmann Method,* Proceedings of the ASME Turbo Expo 2012, Copenhagen, Denmark.

[27] M. Zangeneh and M. de Maillard, *Optimization of Fan Noise by Coupling 3D Inverse Design and Automatic Optimizer,* Proceedings of Fan 2012, Senlis, France.

[28] Amazon Elastic Compute Cloud (EC2) Documentation, http://aws.amazon.com/documentation/ec2/